Research Square

Preprints are preliminary reports that have not undergone peer review.
They should not be considered conclusive, used to inform clinical practice,
or referenced by the media as validated information.

Quantum Molecular Resonance and a blood-derived secretome remodel the DNA methylome of oxidatively stressed human retinal pigment epithelium

Domenico Mordà
University of Messina
Simona Alibrandi
University of Messina
Concetta Scimone
University of Messina
Angela D'Ascola
University of Messina
Federica Aliquò
University of Messina
Giorgia Abate
University of Messina
Sergio Zaccaria Scalinci
University of Bologna
Rosalia D'Angelo
rdangelo@unime.it

University of Messina
Antonina Sidoti
University of Messina
Luigi Donato
University of Messina

Research Article

Keywords: Quantum Molecular Resonance, DNA methylation, whole-genome bisulfite sequencing, retinal pigment epithelium, age-related macular degeneration, oxidative stress, regression to the mean, NRF2 antioxidant response, patient blood-derived secretome, multi-omics integration

Posted Date: November 23rd, 2026

DOI: https://doi.org/10.21203/rs.3.rs-11154220/v1

License: This work is licensed under a Creative Commons Attribution 4.0 International License.
Read Full License

Additional Declarations: No competing interests reported.

Quantum Molecular Resonance and a blood-derived secretome remodel the DNA methylome of oxidatively stressed human retinal pigment epithelium

Domenico Mordà[1,2,3], Simona Alibrandi[1,2], Concetta Scimone[1], Angela D'Ascola[4], Federica Aliquò[1], Giorgia Abate[1,6], Sergio Zaccaria Scalinci[5], Rosalia D'Angelo[1,*], Antonina Sidoti[1] and Luigi Donato[1,2]

[1] Department of Biomedical and Dental Sciences and Morphofunctional Imaging, Division of Medical Biotechnologies and Preventive Medicine, University of Messina, 98125 Messina, Italy

[2] Department of Biomolecular Strategies, Genetics and Avant-Garde Therapies, Euro-Mediterranean Institute of Science and Technology (I.E.ME.S.T.), 90139 Palermo, Italy

[3] Department of Veterinary Sciences, University of Messina, 98125 Messina, Italy

[4] Department of Clinical and Experimental Medicine, University of Messina, 98125 Messina, Italy

[5] Department of Medical and Surgical Sciences, University of Bologna, 40121 Bologna, Italy

[6] Department of Chemical, Biological, Pharmaceutical and Environmental Sciences, University of Messina, 98166 Messina, Italy

* Correspondence: rdangelo@unime.it

Running title: QMR remodels the oxidatively stressed RPE methylome

ABSTRACT

Background. Oxidative damage to the retinal pigment epithelium (RPE) drives age-related macular degeneration, whose atrophic form has no disease-modifying therapy. We have mapped the response of oxidatively stressed RPE to two non-pharmacological, cell-free interventions — Quantum Molecular Resonance (QMR) electrotherapy and a patient blood-derived secretome — across seven RNA layers; the DNA-methylation layer, the only heritable one, had not been examined. We profiled it by whole-genome bisulfite sequencing of 28 libraries from ARPE-19 cells under tert-butyl hydroperoxide at 24 and 72 hours, modelling methylation in 1-kb tiles (2.3 million analysable) with edgeR. Treatment contrasts were fully replicated; the unstressed arm was sequenced once, so a restoration index built on it was tested against an empirical null: one untreated control replicate was withheld and scored as if it were a treatment, giving the value the index takes when nothing was done.

Results. Global CpG methylation was invariant (76.2–76.9%); all effects were therefore focal. Differential methylation was combination-dominant and peaked at 72 hours (combination, 41 regions versus the stressed control; secretome, 24; QMR, 9), distinct from each single agent, enriched in CpG-island promoters and converging on *OGG1* and *ALDH1A3*. Oxidative stress hypermethylated the NRF2 antioxidant promoter battery and hypomethylated *NFKB1* and *NLRP3*; at 72 hours QMR and the secretome returned it to baseline, the combination only partially. The index placed 85–88% of stress-responsive regions closer to baseline, apparently far above chance, yet the untreated control scored equally well (treatment minus control −0.5 percentage points, 95% CI −3.4 to +2.4, P = 0.72): regression to the mean, not treatment effect. A second pipeline agreed in direction at 9 of 11 antioxidant-panel genes (sign test P = 0.033). In the matched

transcriptome the combination induced the NRF2 antioxidant programme (*HMOX1* +3.1 log2 fold change), whereas promoter methylation and expression were uncorrelated (Spearman r = 0.06; 95% CI −0.19 to 0.30; 73 genes).

Conclusions. DNA methylation is a focally remodelled layer of QMR- and secretome-mediated RPE cytoprotection, decoupled from transcription and therefore a parallel rather than upstream stratum. Apparent restoration toward baseline does not survive an empirical null — a caution for any perturbation–intervention methylome study built on an unreplicated reference.

Keywords: Quantum Molecular Resonance; DNA methylation; whole-genome bisulfite sequencing; retinal pigment epithelium; age-related macular degeneration; oxidative stress; regression to the mean; NRF2 antioxidant response; patient blood-derived secretome; multi-omics integration.

1. BACKGROUND

1.1. The retinal pigment epithelium under oxidative siege

Age-related macular degeneration (AMD) is the leading cause of irreversible central-vision loss in industrialized countries, affecting more than 190 million people worldwide and projected to reach 288 million by 2040 [1]. No disease-modifying therapy is approved for the prevalent atrophic ("dry") form, and anti-VEGF biologics address only the neovascular endpoint without halting the underlying degeneration [2]. AMD pathobiology converges on the progressive dysfunction and death of the retinal pigment epithelium (RPE), a polarized monolayer of post-mitotic, melanin-containing cells that sustains photoreceptor survival through phagocytosis of shed outer-segment membranes, vectorial transport, maintenance of the outer blood–retinal barrier, retinoid recycling, and secretion of trophic factors such as PEDF and VEGF-A [3]. The cumulative oxidative burden imposed by this metabolic workload renders the RPE uniquely vulnerable to mitochondrial dysfunction, proteostatic failure, Bruch's-membrane deterioration and chronic para-inflammation, the convergent axes of AMD [4,5]. Exposure of human ARPE-19 cells to tert-butyl hydroperoxide (tBHP) faithfully reproduces this oxidative milieu — eliciting mitochondrial damage, NF-κB and p38/MAPK activation, glutathione depletion and the transcriptional hallmarks of AMD-associated RPE degeneration — and is the reference platform for mechanistic studies of RPE cytoprotection [6].

1.2. DNA methylation: a redox-responsive regulatory layer

Beyond genetic risk, AMD has a substantial epigenetic component. DNA methylation — the covalent modification of cytosine, predominantly at CpG dinucleotides — controls RPE identity and the expression of stress-response, complement and angiogenic genes; promoter and CpG-island methylation generally represses transcription, whereas gene-body methylation tracks active elongation [7]. Whole-genome and locus-specific studies of AMD donor RPE have identified disease-associated differentially methylated regions (e.g. at *SKI*, *GTF2H4*, *TNXB*, the glutathione-S-transferase cluster and *IL17RC*) and accelerated epigenetic ageing [8,9,10]. Crucially, the methylome is not a static blueprint but a redox-responsive layer: reactive oxygen species (ROS) deplete the S-adenosyl-methionine (SAM) pool that DNA methyltransferases (DNMT1/3A/3B) require, oxidize 5-methylcytosine, and impair the ten-eleven translocation (TET) dioxygenases that drive active demethylation, together producing both global and focal methylation change [11,12]. Oxidative stress therefore does not merely damage the RPE — it reprograms its epigenome —

raising the possibility that an intervention able to *restore* a physiological methylation landscape could be disease-modifying. Because DNA methylation can act upstream of transcription, it is often proposed to underpin transcriptomic reprogramming in candidate RPE therapies — a hypothesis we test directly here by integrating the methylome with the matched transcriptome.

1.3. Two cell-free, non-pharmacological strategies: biophysical resonance and a blood-derived secretome

Two conceptually distinct strategies have emerged to protect stressed RPE without cells or small-molecule drugs. Quantum Molecular Resonance (QMR) is a biophysical electrotherapy that delivers low-power, high-frequency electric fields (a 4-MHz fundamental with 8–64-MHz harmonics) calibrated to transfer energy to molecular bonds without thermal damage; QMR and related low-frequency/pulsed electromagnetic fields exert cytoprotective, anti-inflammatory and pro-regenerative effects across many cell systems [13,14], modulate gene expression in RPE [14], and can alter DNA methylation and DNMT expression [15]. Patient blood-derived (PBD) secretomes — the soluble growth factors, cytokines, extracellular vesicles and microRNAs (miRNAs) released by activated autologous blood, conceptually related to platelet-rich plasma and conditioned serum — recapitulate much of the trophic, anti-inflammatory and antioxidant benefit of cell therapy without the cells; such preparations protect ARPE-19 from oxidative and phototoxic injury, restore mitochondrial viability and promote cytoprotective autophagy [16,17], and blood-serum eye-drops rescue retinal neurons in vivo [18]. Whether either modality — and especially their combination — can remodel the genome-wide methylome of oxidatively stressed human RPE has never been examined.

1.4. A multi-omics atlas and the missing epigenetic stratum

On a single ARPE-19 oxidative-stress cohort we have assembled a multi-layer molecular map of QMR and PBD-secretome action, establishing that QMR restores stress-deregulated microRNAs (anti-pyroptotic miR-590-3p, anti-inflammatory miR-146a-5p) while the secretome induces regenerative miRNAs [19], and that QMR is the dominant driver of non-coding-transcriptome variance, engaging *circASPH*/*circCRIM1* competing-endogenous-RNA axes [20]. Four further RNA-level analyses of the same cohort — bulk mRNA reprogramming of antioxidant defenses and proteostasis, the oxidative chimeric-transcript burden, expressed-variant profiling, and the epitranscriptome together with A-to-I editing — are companion manuscripts in preparation by the same authors and are not cited here. Together these seven RNA-level layers describe the abundance, stability, non-coding architecture, structural fidelity, allelic expression and chemical modification of the transcriptome — yet none addresses the DNA-level epigenetic state itself.

Here we close that gap with whole-genome bisulfite sequencing of the same experimental system, positioning this study as the integrative capstone of the series: it contributes the eighth and only DNA-level layer and, for the first time, relates that layer to the expressed transcriptome and to the convergent gene programs of the preceding seven. Three features distinguish it from the companion analyses, which all interrogate one shared RNA-seq dataset. First, it rests on an independent, newly generated WGBS dataset (28 libraries) rather than a re-reading of the transcriptome. Second, it introduces analyses specific to the heritable epigenome that have no counterpart in the RNA layers: an epigenetic-restoration index together with the empirical null required to interpret it; a two-pipeline (edgeR + CLC) concordance test of the oxidative-stress signature; and a methylation–transcription integration that tests whether the methylome

acts upstream of, or in parallel with, the expression program. Third, it synthesizes the eight layers into a single convergence map of the loci jointly remodeled across DNA methylation and RNA regulation. Concretely, we (i) map the oxidative-stress methylation signature and delimit what an unreplicated baseline allows us to conclude from it; (ii) quantify, with three biological replicates and a count-based GLM, the focal differential methylation induced by QMR, the secretome and their combination; (iii) test an epigenetic-restoration index against an empirical null; (iv) integrate the methylome with the matched transcriptome; and (v) assess concordance with an independently implemented pipeline — thereby defining DNA methylation as a distinct, parallel regulatory stratum of biophysically-assisted, cell-free RPE protection.

2. METHODS

2.1. Cell culture and authentication

Human retinal pigment epithelial cells (ARPE-19; ATCC CRL-2302, Manassas, VA, USA) were cultured in high-glucose DMEM/F-12 (Thermo Fisher Scientific) supplemented with 10% fetal bovine serum, 2 mM L-glutamine and 100 U/mL penicillin–streptomycin, and maintained at 37 °C in a humidified 5% CO_2 atmosphere. Cell-line identity was confirmed by short-tandem-repeat profiling (PowerPlex 10, Promega; >80% concordance) and cultures were verified mycoplasma-free every two months (MycoAlert PLUS, Lonza).

2.2. Oxidative-stress induction

Oxidative stress (OX) was induced with tert-butyl hydroperoxide (tBHP; Sigma-Aldrich) applied continuously from t = 0 at 75 µM — a concentration empirically calibrated by MTT assay to reduce viability by ~50% at 24 h — to model the oxidative milieu of RPE degeneration. Matched cultures without tBHP served as the unstressed baseline (NOX).

2.3. Quantum Molecular Resonance (QMR) treatment

QMR stimulation was delivered with a benchtop QMR generator (Telea Electronic Engineering, Sandrigo, Italy; 230 V, 50/60 Hz, max 250 VA) emitting a multifrequency signal comprising a 4-MHz fundamental and higher-order harmonics from 8 to 64 MHz. Two flat stainless-steel electrodes were inserted at the edge of the 90-mm culture plate until contacting the medium surface; the medium volume was held at 12 mL, yielding an estimated electric-field strength of 1.1 ± 0.2 V/cm 2 mm above the monolayer (validated with Ag/AgCl microelectrodes, n = 3) and a current density of ≈12 mA/cm². Each session lasted 10 min at a nominal power setting of 40 (≈10 W output). Cultures analyzed at 24 h received a single session at t = 0; cultures analyzed at 72 h received three sessions (t = 0, ≈24 h, ≈48 h) to capture cumulative effects. Sham controls underwent identical plate handling and electrode positioning with the device powered off, ensuring blinded handling throughout.

2.4. Patient blood-derived (PBD) secretome

The PBD secretome was prepared from peripheral venous blood collected from adult donors under written informed consent and institutional ethics approval (Ethics Committee of A.O.U. G. Martino, Approval No. 858, 23 June 2017). Blood was collected into sodium-citrate tubes, activated with $CaCl_2$ (final 20–25 mM) at 37 °C for 1 h followed by overnight incubation at 4 °C; the fibrin clot was removed by centrifugation (2,000–

3,000 × g, 10 min); the clarified supernatant was filtered (0.22 µm), quantified by BCA assay, aliquoted and stored at −80 °C. For treatment, thawed aliquots were applied at 50% v/v in fresh culture medium. The combination arm (QMR+SEC) received both interventions on the schedules above.

2.5. Experimental design and replication

The experiment was designed in biological triplicate for every treatment×oxidative-condition×time cell. The 28 WGBS libraries analysed here comprise the oxidatively stressed arm (CTRL, QMR, SEC, QMR+SEC × 24 h and 72 h) in three biological replicates per condition×time — eight groups × three replicates minus one, because CTRL at 24 h has n = 2, giving 23 libraries — distributed across three experimental batches (R1, R2, R3) with one replicate per batch in each group so that batch was balanced across treatments; and the unstressed (NOX) baseline arm, complete at 72 h for all four conditions and present for the control at 24 h. The unstressed arm was sequenced in batch R1 only: WGBS libraries for replicates 2 and 3 were generated for the oxidatively stressed arm exclusively, leaving the unstressed baseline unreplicated and confined to a single batch. All analyses involving it are reported as exploratory (§2.10). A further stressed control at 8 h was sequenced in batch R1 but excluded from the present analysis, since neither the corresponding treatment arms nor an unstressed reference were sequenced at that time point. The full sample annotation is provided in Table S1, per-contrast differential-methylation summaries in Tables S2–S2b, and the restoration metrics and their empirical null in Tables S3–S3c.

2.6. DNA extraction, bisulfite sequencing and read processing

Genomic DNA was extracted from matched cell pellets, bisulfite-converted, and used to prepare whole-genome bisulfite sequencing libraries that were sequenced on the Illumina platform in paired-end mode (2 × 150 bp); complete bisulfite conversion was confirmed bioinformatically from non-CpG methylation (>99% across libraries). Reads were quality- and adapter-trimmed with Trim Galore/Cutadapt and assessed with FastQC. Trimmed reads were aligned to the human reference genome GRCh38/hg38 with Bismark v0.24.2 [23] using Bowtie2 [24] in directional mode (--score-min L,0,-0.2, --maxins 500, --no-mixed --no-discordant --dovetail). PCR duplicates were removed with deduplicate_bismark; methylation calls were extracted in comprehensive, non-overlapping mode; and genome-wide per-cytosine reports were generated with coverage2cytosine. Per-library alignment, deduplication, M-bias and conversion metrics were compiled into the quality-control table (Table S1).

2.7. Tile-level methylation matrix

CpG-context cytosines from both strands (autosomes and sex chromosomes; the mitochondrial genome and unplaced contigs excluded) were aggregated into non-overlapping 1-kb genomic tiles, summing methylated (M) and unmethylated (U) read counts; where a per-CpG report was unavailable or malformed, identical counts were derived from the genome-wide all-context (CX) report restricted to CG context (verified to reproduce the canonical ~76.5% global CpG methylation). Tiles covered by ≥10 reads in every oxidatively stressed sample were retained (2,304,782 tiles). Tile methylation level was computed as $\beta = (M + 0.5)/(M + U + 1)$.

2.8. Multivariate analysis

Principal-component analysis was performed by singular-value decomposition of the sample-mean-centred β matrix restricted to the 50,000 most variable tiles. Sample relationships were summarized by Pearson correlation and average-linkage hierarchical clustering on 1 − r distances.

2.9. Differential methylation

Differential methylation was tested with the edgeR generalized-linear-model framework for bisulfite-sequencing count data [25,26]. For each tile, methylated and unmethylated counts were entered per sample; a sample-level design ~0 + group + batch (group = condition×time, eight levels; batch = R1/R2/R3) was expanded with modelMatrixMeth to fit a per-sample coverage intercept together with group- and batch-specific methylation effects. Dispersions were estimated with estimateDisp and a quasi-likelihood negative-binomial GLM was fitted (glmQLFit, robust). Treatment effects were tested with quasi-likelihood F-tests for the contrasts QMR, SEC and QMR+SEC versus CTRL within each time point; the combination-versus-single-agent contrasts (QMR+SEC vs QMR; QMR+SEC vs SEC); and the 72 h-versus-24 h time contrasts. P-values were adjusted genome-wide by the Benjamini–Hochberg method. A tile was called a DMR at FDR < 0.05 and $|\Delta\beta| \geq 0.10$ (group-mean methylation difference computed from the pooled counts), and adjacent same-direction DMR tiles (≤1 kb apart) were merged into regions.

2.10. Oxidative-stress signature and epigenetic restoration

Because the unstressed arm is unreplicated and entirely contained within batch R1, oxidative state and batch are not separable in this contrast and no calibrated error rate can be obtained; this analysis is accordingly exploratory and its outputs are reported as effect sizes and directions rather than as error-controlled discoveries. Oxidative-stress-responsive tiles (OS-DMRs) were defined on effect size alone, as tiles with $|\beta(\text{CTRL,OX}) - \beta(\text{CTRL,NOX})| \geq 0.10$ whose direction was corroborated within the batch-matched first replicate. For ranking only, the edgeR methylation GLM was additionally fitted across all libraries (sample-level design ~0 + group, group = condition×oxidative-state×time, expanded with modelMatrixMeth; note that no batch term is estimable here) with a common negative-binomial dispersion borrowed across all tiles and from the replicated stressed groups; the resulting nominal p-values are not interpreted as error rates. Direction was checked independently by the within-batch CLC analysis (§2.12). For each treatment X and each OS-DMR, a restoration fraction was computed as $[\beta(\text{CTRL,OX}) - \beta(\text{X,OX})] / [\beta(\text{CTRL,OX}) - \beta(\text{CTRL,NOX})]$, where 1 denotes full normalization toward the unstressed baseline, 0 no change and negative values aggravation. Per treatment×time we report the percentage of OS-DMRs moved toward baseline with its 95% Wilson confidence interval, the median restoration fraction (winsorized to [−1, 2]), the fraction fully restored, and the fraction aggravated (Table S3). Because OS-DMRs are selected on an extreme deviation measured against the same single-replicate baseline that forms the denominator, regression to the mean inflates the percentage moved toward baseline and 50% is not the appropriate null. We therefore constructed an empirical null by leave-one-out over the replicated oxidatively stressed control: for each replicate in turn, the signature was recomputed by the identical edgeR procedure from the remaining control replicates, and the withheld replicate — untreated by definition — was scored exactly as a treatment, with treatments from the same replicate scored on the same regions. The difference between each treatment and the withheld control was summarized across folds by a one-sample t-test.

2.11. Annotation, enrichment and cross-omics integration

DMRs were annotated against UCSC hg38 RefSeq gene models (collapsed per gene symbol), TSS±2-kb promoters and CpG islands (cpgIslandExt), and assigned to the nearest transcription start site. Genes with a DMR overlapping their promoter or within 5 kb of their TSS were submitted to over-representation analysis with Enrichr [27] against GO Biological Process, KEGG, Reactome, MSigDB Hallmark, GWAS Catalog and Jensen DISEASES. For cross-omics integration, promoter methylation and the restoration metrics were quantified at a curated panel of genes implicated in the companion transcriptomic layers (NRF2/antioxidant axis, mitochondrial surveillance, AMD/RPE markers, structural-fidelity chimera nodes, non-coding-RNA hosts) and the DNA-methylation machinery.

2.12. Concordance analysis with an independently implemented pipeline (CLC Genomics Workbench)

The first replicate was re-processed with CLC Genomics Workbench (Bisulfite Sequencing module) against the curated GRCh38 (hg38, no-alt) reference with Ensembl v113 annotation. Differential methylation was called "over annotations" for CG, CHG and CHH contexts, comparing oxidatively stressed versus unstressed states (within batch R1) and each treatment versus the stressed control, yielding per-region case/control methylation levels, coverage and nominal p-values. This analysis uses the same sequencing libraries as the primary pipeline and therefore tests analytical, not biological, reproducibility. Its p-values are computed without biological replication (the workbench treats the two sequencing lanes as samples) and without correction for multiple testing; across the 16 CG contrasts, >99.9% of the ~110,000 annotated regions per contrast reach nominal $p < 0.05$, so these p-values carry no discriminative information and are neither used nor reported. Concordance was assessed on direction and effect size only. Contrasts were taken in the *_OX_vs_* orientation, so that case − control equals the oxidative-stress or treatment-induced change; note that the reciprocal exports are not sign-inversions of one another, as the two runs define different region sets. Region-level results were intersected with the pre-specified gene panel; for each gene, direction was summarized both by the single most extreme region and by the mean across all regions of that gene, and the two summaries were compared to confirm that concordance does not depend on the region-selection rule. Between-pipeline directional agreement across the antioxidant panel was tested by an exact sign test (Tables S5, S5b).

2.13. Integration with the matched transcriptome

The matched RNA-seq cohort of the companion series (GEO GSE328981) — the same ARPE-19 model, treatment arms, oxidant and 24 h/72 h sampling, with an additional 8 h arm not used here — was retrieved as the processed linear expression matrix (78,932 genes). Group-mean expression was computed per condition×oxidative-state×time (averaging biological replicates across library preparations), and $\log_2$ fold changes were derived for each treatment versus the oxidative-stress control and for oxidative stress versus the unstressed baseline (pseudocount 1). For each gene, the treatment-induced promoter methylation change (TSS±2 kb, from the tile matrix) was related to the corresponding expression $\log_2$ fold change, and the methylation–expression association was quantified by Spearman correlation across the antioxidant/AMD/companion-layer gene panel, with confidence intervals from the Fisher z-transform (Table S6). The antioxidant transcriptional induction was confirmed robust within each library-preparation subset.

2.14. Software and reproducibility

Trim Galore/Cutadapt, FastQC, Bismark v0.24.2 and Bowtie2 (read processing and methylation calling); R 4.x with edgeR 4.10.1, limma 3.68.4 and data.table; Python 3.12 with NumPy, pandas, SciPy, scikit-learn, Matplotlib and seaborn (matrix construction, multivariate analysis, restoration, annotation, figures); CLC Genomics Workbench (concordance analysis); Enrichr (enrichment). Analysis scripts and intermediate tables are available from the corresponding author on reasonable request.

3. RESULTS

3.1. A deep, high-quality WGBS resource with three biological replicates per stressed condition

The factorial design and its replication are given in §2.5; in brief, the oxidatively stressed arm carries three independent biological replicates per condition and time point, batch-balanced and modeled explicitly, while the unstressed arm was sequenced once (Figure 1; Table S1). The present analysis comprised 28 WGBS libraries that fully cover the oxidatively stressed arm in biological triplicate (the single exception being CTRL at 24 h, n = 2) and the unstressed baseline arm — complete at 72 h for all four conditions and for the control at 24 h. The WGBS experiment sequenced the unstressed arm in a single biological replicate (batch R1): replicates 2 and 3 were generated for the oxidatively stressed arm only. Every comparison involving the unstressed baseline is therefore unreplicated, and is reported throughout as exploratory (§3.4, §2.10); its direction — but not a calibrated significance level — is corroborated within batch R1 by an independently implemented pipeline (§3.6).

All libraries passed stringent quality control (Figure 1; Table S1). Bisulfite-conversion efficiency, estimated from non-CpG (CHH) methylation, was 98.9–99.6%; bisulfite-mapping efficiency was 84.2–88.3%; and post-deduplication depth reached 230–246 million read pairs (≈88–97× median 1-kb-tile coverage) for the deeply sequenced first batch and 100–180 million pairs (≈40–73×) for the additional replicates. Methylation was confined to the CpG context (76.2–76.9%), with negligible CHG/CHH methylation (≤1.1%), confirming both efficient conversion and a canonical somatic methylome. Collapsing CpG cytosines into 1-kb tiles yielded 2,881,748 covered tiles genome-wide; requiring ≥10× coverage in every oxidatively stressed sample retained **2,304,782 analysable tiles**, a fully observed matrix used for all quantitative analyses.

3.2. The RPE methylome is globally invariant; oxidative stress and treatment act focally

Global CpG methylation was remarkably constant across every condition and time point (76.2–76.9%; Figure 2a), excluding any coordinated genome-wide hyper- or hypo-methylation in response to oxidative stress or treatment. The stability has a simple arithmetic explanation rather than a compensatory one: the differentially methylated regions number in the tens against 2.3 million analysable tiles, so even complete inversion at every one of them would move the genome-wide mean by less than 0.01 percentage points. No offsetting counter-shift elsewhere in the genome is required, or detectable. Principal-component analysis of the most variable tiles recovered a diffuse structure (PC1 8.4% and PC2 5.7% of the total variance) whose dominant axis separated the unstressed baselines from the oxidatively stressed samples, with replicate batch contributing additional technical variance within the stressed arm (Figure 2b,c). The small fraction of variance captured by any single component, together with the invariant global methylation, indicates that the biologically meaningful signal resides in discrete, focal regions rather than in a global shift — the regime

in which replicate-based, region-level differential testing is essential and in which simple summary metrics are uninformative.

3.3. The combination of QMR and secretome produces the most extensive, synergistic focal differential methylation

We tested differential methylation with the edgeR generalized-linear-model framework for bisulfite-sequencing counts, which models the methylated and unmethylated read counts per sample, accommodates biological-replicate variability through an empirical-Bayes negative-binomial dispersion, and adjusts for batch (common dispersion 0.0057, reflecting tight replicate consistency). Defining DMRs as tiles at false-discovery rate (FDR) < 0.05 with an absolute group-mean methylation difference $|\Delta\beta| \geq 0.10$, treatment effects were focal, time-dependent and combination-dominant (Figure 3a; Table 1). At 24 h, QMR, secretome and the combination produced 18, 15 and 21 DMRs, respectively. By 72 h the responses diverged sharply: QMR+SEC produced 41 DMRs versus 24 for the secretome and 9 for QMR alone. The combination was also tested directly against each single agent — that is, QMR+SEC versus QMR and QMR+SEC versus the secretome, asking which tiles differ between the combined and the single treatment rather than against the stressed control. These contrasts yielded 25 and 25 DMRs at 72 h (10 and 17 at 24 h): the combination is therefore not simply the sum of its parts but occupies a distinct methylation state, the signature of a synergistic program rather than simple additivity, and consistent with the priming model in which QMR conditions the cell to integrate paracrine secretome signals. DMRs were balanced between gains and losses of methylation (QMR+SEC at 72 h: 19 hyper-, 22 hypo-methylated) and were strongly enriched in CpG-island promoters (Figure 3b), the compartment in which methylation most directly governs transcription.

The combination DMRs converged on biologically coherent nodes of RPE oxidative biology: retinoid metabolism (*ALDH1A3*, a hyper-methylated CpG-island promoter, $\Delta\beta = +0.30$), mitochondrial cytochrome-c-oxidase assembly (*SCO1*), the selenoprotein antioxidant *SELENOF*, the lysosomal/antioxidant *CSTB*, the chaperone *DNAJB1* and the innate-immune sensor *NOD1*. QMR alone selectively targeted the master oxidative-DNA-damage-repair gene *OGG1* (8-oxoguanine DNA glycosylase) and the prostacyclin synthase *PTGIS*, whereas the secretome targeted inflammatory/signaling loci (*JAK1*, *NCOA3*). Consistent with these assignments, over-representation analysis linked QMR DMR genes to base-excision/oxidative-DNA-damage repair and combination DMR genes to selenocompound metabolism and de-novo post-translational protein modification (the latter at FDR = 0.018).

3.4. An epigenetic-restoration index does not survive its own empirical null

To define the oxidative-stress methylation signature we contrasted the stressed and unstressed control with the edgeR GLM (dispersion borrowed across tiles and from the replicated stressed groups; §2.10). Because the unstressed arm is unreplicated, this contrast cannot support calibrated error rates, and we treat it as exploratory throughout. We therefore define oxidative-stress-responsive regions (OS-DMRs) on effect size ($|\Delta\beta| \geq 0.10$), using the model output for ranking only: 162 OS-DMRs at 24 h and 236 at 72 h, predominantly hypermethylated (72 h: 179 of 236, 76%), consistent with the antioxidant-promoter hypermethylation described below, while the broader sub-threshold shift (~1.3×10^5 tiles at $|\Delta\beta| \geq 0.10$) was bidirectional. The unstressed libraries are moreover confined to batch R1; oxidative state and batch are therefore not

separable in this contrast (§2.10). The direction of the signature was reproduced within batch R1 by an independently implemented pipeline (§3.6).

The restoration fraction (§2.10) measures how much of the stress-induced deviation a treatment reverses. All three interventions moved the methylome toward the unstressed state at the majority of regions: 85.2–86.4% at 24 h and 86.0–87.7% at 72 h, with a median reversal of 33–44% of the stress-induced shift (Table S3; an independent reimplementation of the pipeline reproduced these values to within one percentage point). Compared against the 50% expected by chance this appears decisive. That comparison, however, is invalid here, because OS-DMRs are selected on an extreme deviation measured against a single-replicate baseline that also forms the denominator of the fraction, regression to the mean drives the index above 50% even in the absence of any treatment effect.

We therefore built an empirical null from the data themselves. The oxidatively stressed control is replicated (three biological replicates at 72 h, two at 24 h), so the signature can be recomputed by the identical edgeR procedure with one control replicate withheld, and that withheld replicate — which received no treatment — scored exactly as if it were a treatment; treatments from the same replicate are scored on the same regions (§2.10). An untreated control replicate restores the methylome as fully as any treatment**.** Across five folds and three interventions the difference between treatment and untreated control was −0.54 percentage points on average (95% CI −3.4 to +2.4; t = −0.36, P = 0.72; 6 of 15 comparisons positive), and no arm separated from the null (QMR −1.0, secretome −2.0, combination +1.3 points; Figure 4). The null itself ranged from 74.6% to 96.7% depending only on which replicate was withheld — a 22-point spread that brackets the 85–88% obtained from the full data.

The restoration index therefore measures which sample happens to serve as the reference, not what the treatment did, and we report it as a negative methodological result. This does not affect the treatment contrasts of Section 3.3, which are fully replicated, batch-adjusted and independent of the unstressed baseline.

3.5. The methylome converges on the QMR-responsive antioxidant and AMD gene program

We integrated the methylome with the seven companion RNA layers by quantifying promoter methylation at the genes those layers had implicated (Figure 5; Table 2). The result was a coherent, directionally interpretable cross-omics map. Oxidative stress hyper-methylated the promoters of the NRF2/antioxidant battery — *GCLC* (Δβ = +0.056 at 72 h), *HMOX1* (+0.054), *GCLM* (+0.041), *TXNRD1*, *PRDX1*, and the glutathione-S-transferases *GSTM1/GSTM5* (up to +0.10 at 24 h) — a configuration predicted to repress antioxidant defense. Conversely, stress hypo-methylated pro-inflammatory and inflammasome loci (*NFKB1* −0.054, *NLRP3* −0.051), predicted to de-repress inflammation, and perturbed the methylation machinery itself (*DNMT1* −0.076, *DNMT3B* +0.054, *IDH2* +0.058). AMD-relevant loci followed suit (complement *CFH* +0.054, *HTRA1* +0.045), as did the host genes of the QMR-responsive non-coding transcripts identified previously (*NEAT1* −0.052, *BASP1* +0.052, *ASPH* +0.043) and the chimera node *CTDNEP1* (+0.045).

Treatment reversed the antioxidant-promoter hypermethylation, but unevenly across arms: averaged over the NRF2/antioxidant panel at 72 h, promoter methylation rose from the unstressed baseline (β = 0.631) under oxidative stress (0.646) and was returned to or below baseline by QMR (0.627) and by the secretome (0.630), whereas the combination reversed it only partially (0.641) (Figure 5b). At 24 h the ordering differed

again, the secretome exceeding the stressed control (0.641 versus 0.634) while QMR (0.628) and the combination (0.628) fell between baseline and stress. Aggregate antioxidant-promoter demethylation under treatment is therefore a real but arm- and time-dependent effect — and, notably, the combination, the arm with the most extensive focal differential methylation, is not the one that normalizes this panel most. However, as the matched-transcriptome integration below shows (Section 3.7), promoter methylation and the acute antioxidant transcriptional response are largely decoupled; we therefore interpret coordinated antioxidant-promoter demethylation as a parallel epigenetic correlate of the cytoprotective program rather than its strict upstream cause, and DNA methylation as an independent regulatory stratum of the multi-omics response.

3.6. Concordance with an independently implemented pipeline

To test whether the oxidative-stress signature depends on the analytical pipeline, and to compare the stressed and unstressed states within a single batch, we re-processed the first replicate with an independently implemented workflow — CLC Genomics Workbench differential methylation over annotations (Ensembl v113; CG/CHG/CHH contexts) (Figure 6; Tables S5, S5b). Two properties of that workflow frame what it can establish. It uses the same sequencing libraries as the primary analysis, so it tests analytical rather than biological reproducibility; and its region-level p-values are computed without biological replication and without correction for multiple testing, so that essentially every annotated region reaches nominal significance (>99.9% of ~110,000 regions at $p < 0.05$, in each of the 16 contrasts examined). We therefore assess concordance on direction and effect size only, and report no p-values from this pipeline.

On that basis the agreement is strong. Of the 19 genes of the pre-specified NRF2/antioxidant panel, 11 are annotated in the CLC CG output. All 11 are hypermethylated under oxidative stress in the CLC analysis, and 9 of the 11 agree in direction with the primary WGBS analysis (sign test $P = 0.033$). The two exceptions are *GPX1* and *GSTM5*, scored as hypomethylated by the primary pipeline ($\Delta\beta = -0.008$ and -0.078) and as hypermethylated by CLC ($\Delta = +0.13$ and $+0.39$); *GSTM5* is the largest single discrepancy in the panel. Concordance is unchanged whether each gene is summarized by its most extreme CLC region or by the mean across all of its regions, so it does not depend on the region-selection rule. The figure is the unselected result across the entire pre-specified antioxidant panel: no gene was dropped for disagreeing. Among treatment-responsive loci, *OGG1* is the most striking: in the QMR contrast at 72 h it shows a methylation difference of $\Delta = +0.57$ over a single 1-kb region (chr3:9,749,001–9,750,000), ranking 16th of 113,385 regions genome-wide (top 0.014%). Two pipelines that differ in region definition, statistical model and annotation source thus recover the same directional antioxidant/AMD programme from these libraries.

3.7. Integration with the matched transcriptome: combination-driven antioxidant induction without a methylation counterpart

To position the methylome relative to gene expression, we integrated it with the matched RNA-seq cohort of the companion series (GEO GSE328981) [32] — the same ARPE-19 model, treatment arms, oxidant and 24 h/72 h sampling, the RNA-seq series additionally including an 8 h arm not sequenced here, and two results emerged (Figure 7). First, in the transcriptome the combination coordinately induced the NRF2/antioxidant program under oxidative stress at 72 h — *HMOX1* (+3.1 $\log_2$FC versus the oxidative-stress control), *GCLM* (+1.1), *NQO1* (+1.0), *TXNRD1* (+0.9), *TXN* (+0.8), *GSR* (+0.5), *SRXN1* (+0.5), *GCLC* (+0.4) and *NFE2L2* (+0.4) —

an induction reproduced independently within each library-preparation subset — a control that rules out a batch artifact in the transcriptomic comparison — and that exceeded either single agent, although the secretome alone accounted for much of it (e.g. *HMOX1* +1.9), whereas QMR alone was weak or slightly negative for these genes, consistent with a priming role, providing transcriptional confirmation of combination-driven cytoprotection (Figure 7a). Second, across the companion-gene panel, promoter methylation change and expression change were uncorrelated (Spearman r = 0.06, p = 0.64, 95% CI −0.19 to 0.30, n = 73 genes, for the combination at 72 h; $|r| \leq 0.31$ across all contrasts and time points; Figure 7b). The confidence interval excludes any strong association but is compatible with a weak one, so this is evidence against methylation acting as the proximal switch, not proof of complete independence. Two features make the decoupling concrete. The genes concerned are not transcriptionally silent — *HMOX1*, *GCLM* and *NQO1* are among the most strongly induced in the cohort — so the absence of correlation is not a failure to detect expression. And the mismatch is one of magnitude and sign rather than of ordering: *HMOX1* gains 3.1 $\log_2$ units of expression against a promoter methylation change of less than one percentage point, while genes whose promoters move most are not those whose expression moves most. Because both layers were sampled at the same two time points, we cannot exclude that a methylation response simply lags transcription and would emerge beyond 72 h; what the data exclude is that promoter methylation *precedes and drives* the acute induction. DNA methylation therefore operates as a parallel, slower-acting regulatory stratum rather than the proximal switch for these inducible stress genes — the expected behaviour for inducible, low-CpG stress promoters [33], and consistent with integrative methylation–transcription analyses in AMD tissue [34,35].

4. DISCUSSION

This study adds the DNA-methylation layer to a multi-omics dissection of how QMR and a PBD secretome protect oxidatively stressed human RPE. Four findings stand out. First, the RPE methylome is globally invariant under oxidative stress and treatment, so the action of all interventions is focal and regulatory, concentrated in CpG-island promoters. Second, against this stable background, replicate-based statistical testing shows that QMR and the secretome induce focal differential methylation that is most extensive in combination and at the late (72 h) time point, and that is statistically distinct from either single agent — a synergistic epigenetic program. Third, an epigenetic-restoration index places ~85–88% of the oxidative-stress signature closer to the unstressed baseline, but an untreated control replicate scores just as highly, so the index reflects regression to the mean rather than treatment — a negative result with methodological implications beyond this dataset. Fourth, and most importantly, these methylation changes are not random: they converge, in a directionally coherent manner reproduced by a second analytical pipeline, on the NRF2/antioxidant, mitochondrial, retinoid, inflammatory and AMD-risk loci that define the downstream transcriptomic program.

4.1. A redox–methylation vicious cycle and how QMR breaks it

The convergence on the antioxidant response is the conceptual centerpiece. Oxidative stress hypermethylated the promoters of *GCLC*, *GCLM*, *HMOX1*, *TXNRD1*, *PRDX1* and the glutathione-S-transferases — a configuration expected to silence the antioxidant defense of the cell precisely when it is most needed. This is mechanistically consistent with the established redox–epigenome crosstalk, in which

ROS deplete the SAM methyl-donor pool, inhibit TET-mediated demethylation, and redistribute DNMTs, biasing CpG islands toward hypermethylation [11,12]; the net effect is a self-reinforcing vicious cycle in which oxidative damage epigenetically disables the very NRF2-driven program (*GCLC*/*GCLM* for glutathione synthesis, *HMOX1*, *TXNRD1*/*PRDX1* for thiol redox) that would otherwise resolve it — the KEAP1–NRF2 axis that normally licenses this battery [28] and the glutathione-synthetic step it controls [29]. QMR and the secretome reversed this hypermethylation, returning aggregate antioxidant-promoter methylation to or below baseline at 72 h, while the combination did so only partially — so the arm with the most extensive focal remodelling is not the one that normalizes this panel best. In the matched transcriptome, nonetheless, the combination coordinately induced these antioxidant genes (*HMOX1*, *GCLM*, *NQO1*, *TXNRD1*, *GSR*, *GCLC*; Section 3.7). Crucially, however, promoter methylation and expression were largely decoupled at these loci, so we do not interpret antioxidant-promoter demethylation as the proximal cause of induction — which is most plausibly NRF2-driven — but as a parallel relaxation of the epigenetic landscape that may license or help sustain the antioxidant response. Other epigenetic layers not measured here could carry the acute signal instead: histone-tail modifications at antioxidant response elements, and post-transcriptional control by the miRNA programme that the companion small-RNA layer shows to be extensively remodelled in the same cells [19], both act on a timescale compatible with the induction we observe, whereas CpG methylation does not. DNA methylation thus emerges as an independent regulatory stratum, concordantly remodeled with rather than strictly upstream of the transcriptional program, consistent with the documented context-dependence of promoter-methylation control at inducible, low-CpG stress genes [33]. The reciprocal hypomethylation of *NFKB1* and *NLRP3* under stress, and its partial reversal by treatment, is consistent with the coupling of oxidative stress to inflammatory activation in non-neovascular AMD [30] and mirrors the anti-inflammatory miRNA program (miR-146a-5p) reported in the small-RNA layer [19]. The selective DMR at *OGG1* under QMR — which in the second pipeline shows a Δ of +0.57 and ranks in the top 0.014% of regions genome-wide — is mechanistically elegant: by remodeling the methylation of the very enzyme that excises oxidative 8-oxoguanine lesions, QMR may reinforce genome-protective base-excision repair, the pathway recovered by enrichment analysis. The combination's DMRs at *ALDH1A3* (retinaldehyde metabolism, central to the visual cycle and RPE identity) and *SCO1* (cytochrome-c-oxidase assembly) tie the epigenetic response to two hallmark RPE functions, retinoid handling and mitochondrial bioenergetics, the latter echoing the mitochondrial-surveillance signal seen in the expressed-variant layer of the same cohort (manuscript in preparation).

4.2. QMR as a priming stimulus and the logic of combination

Across the series, QMR has behaved as a priming stimulus — the dominant driver of non-coding-transcriptome variance that readies cells to integrate paracrine secretome signals [20]. The methylome data are consistent with and extend this model: QMR alone produced the fewest statistically robust DMRs at 72 h (9) yet the combination produced the most (41) and differed significantly from both single agents. We interpret this as QMR conditioning the chromatin/methylation landscape that the secretome's trophic factors then exploit, so that the two modalities are mechanistically complementary rather than redundant. That the methylome — the most stable and heritable molecular layer — is nonetheless measurably and restoratively remodeled argues that biophysical conditioning reaches the deepest regulatory stratum of the cell. The precise transducer remains to be defined; plausible routes include field effects on intracellular Ca^{2+}

and redox dynamics that feed into one-carbon/SAM metabolism and TET/DNMT activity, a hypothesis our data motivate but cannot yet prove.

4.3. The integrative capstone of the multi-omics atlas: what is new beyond the companion series

This study is the integrative capstone of a multi-omics program, and three features make it a distinct contribution rather than a further instalment. First, it is the only DNA-level layer and the only one built on an independently generated dataset: the seven companion RNA-level analyses all mine a single shared RNA-seq cohort, whereas the methylome reported here is a new 28-library WGBS experiment, so it adds genuinely new measurements rather than a new reading of the same molecules. Second, it contributes concepts that have no equivalent in the RNA layers — a quantitative epigenetic-restoration index with the leave-one-out null needed to interpret it, a two-pipeline concordance test of the stress signature, and a formal methylation–transcription integration. Two of these yield non-obvious results. The restoration index, intuitive and apparently decisive at face value, collapses against its own null, and we report it as a cautionary negative finding rather than as evidence of treatment effect. The integration shows that the benefit of QMR and the secretome is not transmitted through methylation-driven transcription of antioxidant genes (the two layers are decoupled), correcting a tempting but unsupported causal narrative and reframing methylation as an independent stratum. Third, by relating the methylome to the transcriptome and to the marquee genes of every preceding layer (Figure 5), it provides the first cross-layer convergence map of the system, the synthesis that only the final, DNA-level layer can deliver. Together these distinguish the work from the companion papers at the levels of data, methods and conclusions.

Our findings also dovetail with human AMD epigenomics: donor-RPE WGBS and blood/retina studies have reported AMD-associated differential methylation at antioxidant, complement and structural loci [8,9], and our recurrent hits at the glutathione-S-transferase/antioxidant cluster and at *CFH*/*HTRA1* — the latter in a tissue that is a recognised hotspot of complement dysregulation [31] — place the QMR-responsive program squarely within disease-relevant epigenetic space. By adding the genomic/epigenetic stratum to seven RNA layers on one cohort, this work yields an integrated, eight-layer model in which a coordinated cytoprotective response is engaged across complementary, partly independent regulatory strata — focal remodelling of antioxidant-promoter methylation (this study), anti-inflammatory and anti-pyroptotic miRNA programs [19], non-coding ceRNA rewiring [20], and, in companion analyses in preparation, antioxidant mRNA induction, suppression of structural chimeras, mitochondrial-surveillance variants and a selectively remodelled epitranscriptome — rather than propagating from a single upstream switch, as our matched methylation–transcription analysis (decoupled at antioxidant loci) makes explicit. Such multi-layer integration across regulatory strata is rarely available for a candidate therapy and provides an unusually complete mechanistic picture.

4.4. Translational implications

"Epigenetic restoration toward baseline" is an attractive therapeutic endpoint for a degenerative disease in which the aim is not to drive cells to a novel state but to return a stressed epithelium to homeostasis [21,22]. Our results, however, are a caution about how that endpoint is measured: an index of movement toward an unreplicated baseline is dominated by regression to the mean, and only a held-out untreated control reveals it (Section 3.4). We recommend that such indices always be reported against an empirical null of this kind.

QMR and a PBD secretome are non-pharmacological, combinable and (for the secretome) autologous, and the combination's markedly greater focal remodelling supports its further development — though on the aggregate antioxidant-promoter panel the single agents performed at least as well, so which regimen best restores homeostasis is not yet settled. The restoration index we introduce is a transferable readout that could be applied to any perturbation–intervention methylome dataset to benchmark the homeostatic, rather than merely the differential, effect of a treatment.

4.5. Limitations

Several limitations temper interpretation. (i) ARPE-19 is an immortalized line; constitutive methylation features may not fully recapitulate primary RPE or in vivo retina, and validation in primary cultures and donor tissue is warranted. (ii) The unstressed baseline is unreplicated, and this is the principal limitation of the study. The treatment-versus-control comparisons under oxidative stress are fully replicated (three biological replicates, batch-balanced) and support calibrated inference. The WGBS experiment, however, sequenced the unstressed arm in one biological replicate only, all of it within batch R1; replicates 2 and 3 exist for the oxidatively stressed arm alone. Two consequences follow and cannot be removed by analysis. Oxidative state is confounded with batch in this contrast, so the oxidative-stress signature cannot be separated from a batch effect; and the restoration index, which measures movement away from a single-replicate reference at regions selected for their extreme deviation from that same reference, is inflated by regression to the mean by an amount we cannot presently quantify. We therefore report both as exploratory, define OS-DMRs on effect size rather than on a nominal error rate, and rest the biological claim on what does not depend on the baseline replication: the direction of the antioxidant-promoter shift, which a second, independently implemented pipeline reproduces within batch R1 at 9 of 11 genes of the pre-specified antioxidant panel ($P = 0.033$). We quantified both problems directly. Recomputing the signature within batch R1 rather than across batches changes it 2.2-fold (140 versus 304 regions at 24 h), and the restoration index does not exceed a held-out untreated control (Section 3.4). A fully replicated unstressed arm is required before treatment-specific normalization can be claimed. (iii) Replicate batches differed in sequencing depth; we addressed this with a uniform high-coverage tile filter and explicit batch terms in the model, and the residual technical axis is orthogonal to the treatment contrasts. (iv) The model is acute: a single oxidative insult and one or three treatment sessions over at most 72 h. Promoter methylation is a comparatively slow, self-reinforcing mark, and an acute design may capture its earliest movements only; whether the focal remodelling reported here consolidates, reverts or extends under chronic oxidative stress — the situation in AMD — cannot be answered from these data. (v) WGBS cannot distinguish 5-methyl- from 5-hydroxymethyl-cytosine; oxidative-bisulfite or enzymatic-methyl sequencing would resolve the hydroxymethylation contribution, as would native long-read sequencing on the PacBio or Oxford Nanopore platforms, which calls both marks directly without chemical conversion. (vi) The methylation–expression causal link, though directionally consistent across layers and concordant between two analytical pipelines applied to the same libraries, remains correlative, and no functional readout of cytoprotection was collected in this study. Locus-specific epigenome editing (e.g. dCas9–TET1 or –DNMT3A at *GCLC*/*HMOX1*), paired functional assays of viability, redox state and mitochondrial competence, and extended time-courses are required to establish causality and durability.

5. CONCLUSIONS

DNA methylation is an actively QMR-remodeled, independent DNA-level epigenetic layer of the RPE response to oxidative stress. Against a globally invariant methylome, QMR and a PBD secretome focally remodel the methylome — most extensively in combination — at antioxidant, mitochondrial, retinoid and inflammatory loci that converge with the programs of the companion layers. An apparent restoration of the oxidative-stress signature toward baseline does not survive an empirical null and is reported as such. The direction of the antioxidant-promoter effect is reproduced by a second, independently implemented pipeline, and the matched transcriptome shows the combination coordinately inducing the antioxidant program while methylation is remodeled in parallel. As the integrative, DNA-level capstone of an eight-layer multi-omics atlas, this work defines the epigenetic stratum of QMR-plus-secretome conditioning and, in equal measure, the evidentiary standard that claims of epigenetic restoration must meet.

List of abbreviations

AMD: age-related macular degeneration; CGI: CpG island; CI: confidence interval; CLC: CLC Genomics Workbench; DMR: differentially methylated region; FDR: false discovery rate; GLM: generalized linear model; NOX: unstressed (no oxidative stress); OS-DMR: oxidative-stress-responsive differentially methylated region; OX: oxidatively stressed; PBD: patient blood-derived; PCA: principal-component analysis; QMR: Quantum Molecular Resonance; RPE: retinal pigment epithelium; SEC: secretome; tBHP: tert-butyl hydroperoxide; TSS: transcription start site; WGBS: whole-genome bisulfite sequencing.

Declarations

Ethics approval and consent to participate

The study was conducted in accordance with the Declaration of Helsinki and approved by the local Ethics Committee "A.O.U. G. Martino" (date: 23 June 2017; number: 858). Written informed consent was obtained from all blood donors involved in the study. The ARPE-19 cell line is commercially available (ATCC CRL-2302) and its use required no ethics approval.

Consent for publication

Not applicable.

Availability of data and materials

The whole-genome bisulfite sequencing data generated and analysed during the current study, together with the matched bulk RNA-sequencing cohort of the companion series reused here as a processed linear expression matrix for the methylation–transcription integration, are available in the NCBI Gene Expression Omnibus (GEO) repository under accession number GSE328981. Analysis scripts used to construct the tile matrix, call differential methylation, compute the restoration index and generate the figures are available from the corresponding author on reasonable request. All other data supporting the findings are included in the article and its additional files: per-library quality-control metrics (Table S1), per-contrast differential-methylation summaries (Tables S2, S2b), restoration metrics and the empirical null (Tables S3, S3b, S3c), cross-omics promoter methylation (Table S4), the marquee-locus tabulation and two-pipeline concordance (Tables S5, S5b), the methylation–expression integration (Table S6) and the per-contrast region lists.

Competing interests

The authors declare that they have no competing interests.

Funding

This research received no external funding.

Authors' contributions

Conceptualization, LD and SA; methodology, SA; software and formal analysis, LD; validation, DM and SA; investigation, SA; resources, AD and SZS; data curation, RD; writing—original draft, LD; writing—review and editing, SA, GA and DM; visualization, CS, RD and FA; supervision, AS; project administration, LD All authors read and approved the final manuscript.

Acknowledgements

Not applicable.

REFERENCES

1. Wong WL, Su X, Li X, Cheung CM, Klein R, Cheng CY, et al. Global prevalence of age-related macular degeneration and disease burden projection for 2020 and 2040: a systematic review and meta-analysis. *Lancet Glob Health* 2014;2:e106-16.
2. Fleckenstein M, Keenan TDL, Guymer RH, Chakravarthy U, Schmitz-Valckenberg S, Klaver CC, et al. Age-related macular degeneration. *Nat Rev Dis Primers* 2021;7:31.
3. Bhutto I, Lutty G. Understanding age-related macular degeneration (AMD): relationships between the photoreceptor/retinal pigment epithelium/Bruch's membrane/choriocapillaris complex. *Mol Aspects Med* 2012;33:295-317.
4. Kaarniranta K, Uusitalo H, Blasiak J, Felszeghy S, Kannan R, Kauppinen A, et al. Mechanisms of mitochondrial dysfunction and their impact on age-related macular degeneration. *Prog Retin Eye Res* 2020;79:100858.
5. Nita M, Grzybowski A. The role of the reactive oxygen species and oxidative stress in the pathomechanism of the age-related ocular diseases and other pathologies of the anterior and posterior eye segments in adults. *Oxid Med Cell Longev* 2016;2016:3164734.
6. Dunn KC, Aotaki-Keen AE, Putkey FR, Hjelmeland LM. ARPE-19, a human retinal pigment epithelial cell line with differentiated properties. *Exp Eye Res* 1996;62:155-69.
7. Jones PA. Functions of DNA methylation: islands, start sites, gene bodies and beyond. *Nat Rev Genet* 2012;13:484-92.
8. Porter LF, Saptarshi N, Fang Y, Rathi S, den Hollander AI, de Jong EK, et al. Whole-genome methylation profiling of the retinal pigment epithelium of individuals with age-related macular degeneration reveals differential methylation of the SKI, GTF2H4 and TNXB genes. *Clin Epigenetics* 2019;11:6.
9. Oliver VF, Jaffe AE, Song J, Wang G, Zhang P, Branham KE, et al. Differential DNA methylation identified in the blood and retina of AMD patients. *Epigenetics* 2015;10:698-707.
10. Li X, He S, Zhao M. An updated review of the epigenetic mechanism underlying the pathogenesis of age-related macular degeneration. *Aging Dis* 2020;11:1219-34.
11. Niu Y, DesMarais TL, Tong Z, Yao Y, Costa M. Oxidative stress alters global histone modification and DNA methylation. *Free Radic Biol Med* 2015;82:22-8.

12. Kietzmann T, Petry A, Shvetsova A, Gerhold JM, Görlach A. The epigenetic landscape related to reactive oxygen species formation in the cardiovascular system. *Br J Pharmacol* 2017;174:1533-54.

13. Mansourian M, Shanei A. Evaluation of pulsed electromagnetic field effects: a systematic review and meta-analysis on highlights of two decades of research in vitro studies. *Biomed Res Int* 2021;2021:6647497.

14. Oladnabi M, Bagheri A, Rezaei Kanavi M, Azadmehr A, Kianmehr A. Extremely low frequency-pulsed electromagnetic fields affect proangiogenic-related gene expression in retinal pigment epithelial cells. *Iran J Basic Med Sci* 2019;22:128-33.

15. Liu Y, Liu WB, Liu KJ, Ao L, Zhong JL, Cao J, et al. Effect of 50 Hz extremely low-frequency electromagnetic fields on the DNA methylation and DNA methyltransferases in mouse spermatocyte-derived cell line GC-2. *Biomed Res Int* 2015;2015:237183.

16. Suárez-Barrio C, del Olmo-Aguado S, García-Pérez E, de la Fuente M, Muruzabal F, Anitua E, et al. Antioxidant role of PRGF on RPE cells after blue light insult as a therapy for neurodegenerative diseases. *Int J Mol Sci* 2020;21:1021.

17. Suárez-Barrio C, Del Olmo-Aguado S, García-Pérez E, Fernández-Vega-Cueto L, Fernández-Vega Cueto A, Baamonde-Arbaiza B, et al. Plasma rich in growth factors promotes autophagy in ARPE19 cells in response to oxidative stress induced by blue light. *Biomolecules* 2021;11:954.

18. Di Marco S, Riccitelli S, Di Paolo M, Campos E, Buzzi M, Bisti S, et al. Cord blood serum-based eye drops modulate light-induced neurodegeneration in albino rat retinas. *Biomolecules* 2020;10:678.

19. Alibrandi S, Mordà D, Scimone C, D'Ascola A, Aliquò F, Pozzato A, et al. QMR® and patient blood-derived secretome modulate RPE microRNA networks under oxidative stress. *Int J Mol Sci* 2025;26:8614. doi:10.3390/ijms26178614

20. Alibrandi S, Mordà D, Scimone C, D'Ascola A, Aliquò F, Abate G, et al. Quantum molecular resonance and secretome synergistically unlocks a protective ceRNA axis in the human retinal pigment epithelium. *Mol Ther Nucleic Acids* 2026;37:103034. doi:10.1016/j.omtn.2026.103034

21. Horvath S. DNA methylation age of human tissues and cell types. *Genome Biol* 2013;14:R115.

22. Lu Y, Brommer B, Tian X, Krishnan A, Meer M, Wang C, et al. Reprogramming to recover youthful epigenetic information and restore vision. *Nature* 2020;588:124-9.

23. Krueger F, Andrews SR. Bismark: a flexible aligner and methylation caller for Bisulfite-Seq applications. *Bioinformatics* 2011;27:1571-2.

24. Langmead B, Salzberg SL. Fast gapped-read alignment with Bowtie 2. *Nat Methods* 2012;9:357-9.

25. Robinson MD, McCarthy DJ, Smyth GK. edgeR: a Bioconductor package for differential expression analysis of digital gene expression data. *Bioinformatics* 2010;26:139-40.

26. Chen Y, Pal B, Visvader JE, Smyth GK. Differential methylation analysis of reduced representation bisulfite sequencing experiments using edgeR. *F1000Res* 2017;6:2055.

27. Kuleshov MV, Jones MR, Rouillard AD, Fernandez NF, Duan Q, Wang Z, et al. Enrichr: a comprehensive gene set enrichment analysis web server 2016 update. *Nucleic Acids Res* 2016;44:W90-7.

28. Itoh K, Wakabayashi N, Katoh Y, Ishii T, Igarashi K, Engel JD, et al. Keap1 represses nuclear activation of antioxidant responsive elements by Nrf2 through binding to the amino-terminal Neh2 domain. *Genes Dev* 1999;13:76-86.

29. Lu SC. Glutathione synthesis. *Biochim Biophys Acta* 2013;1830:3143-53.

30. Datta S, Cano M, Ebrahimi KB, Wang L, Handa JT. The impact of oxidative stress and inflammation on RPE degeneration in non-neovascular AMD. *Prog Retin Eye Res* 2017;60:201-18.

31. Clark SJ, Bishop PN. The eye as a complement dysregulation hotspot. *Semin Immunopathol* 2018;40:65-74.

32. Alibrandi S, Mordà D, Scimone C, D'Ascola A, Aliquò F, Abate G, et al. Whole-genome bisulfite and RNA sequencing of oxidatively stressed ARPE-19 under Quantum Molecular Resonance and blood-derived secretome. Gene Expression Omnibus. 2026. https://www.ncbi.nlm.nih.gov/geo/query/acc.cgi?acc=GSE328981

33. Thiruvengadam M, Venkidasamy B, Subramanian U, Samynathan R, Shariati MA, Rebezov M, et al. Bioactive compounds in oxidative stress-mediated diseases: targeting the NRF2/ARE signaling pathway and epigenetic regulation. *Antioxidants* 2021;10:1859.
34. Orozco LD, Owen LA, Hofmann J, Stockwell AD, Tao J, Haller S, et al. A systems biology approach uncovers novel disease mechanisms in age-related macular degeneration. *Cell Genomics* 2023;3:100302.
35. Bhargavan B, Chhunchha B, Kubo E, Singh DP. DNA methylation as an epigenetic mechanism in the regulation of LEDGF expression and biological response in aging and oxidative stress. *Cell Death Discov.* 2024;10:296. doi:10.1038/s41420-024-02076-2

Table 1. Treatment-induced differentially methylated regions (DMRs).

DMRs called at FDR < 0.05 and |Δβ| ≥ 0.10 (edgeR quasi-likelihood F-test, batch-adjusted); adjacent same-direction 1-kb tiles merged. Promoter = TSS ± 2 kb; CpG island = UCSC cpgIslandExt overlap.

Contrast	DMRs	Hyper	Hypo	Promoter	CpG island	Genes
QMR vs CTRL @24 h	18	7	11	13	13	16
Secretome vs CTRL @24 h	15	8	7	13	10	16
QMR+Sec vs CTRL @24 h	21	11	10	19	16	23
QMR+Sec vs QMR @24 h	10	3	7	7	7	7
QMR+Sec vs Secretome @24 h	17	7	10	14	13	16
QMR vs CTRL @72 h	9	2	7	6	8	7
Secretome vs CTRL @72 h	24	14	10	17	19	20
QMR+Sec vs CTRL @72 h	41	19	22	25	26	27
QMR+Sec vs QMR @72 h	25	14	11	16	18	18
QMR+Sec vs Secretome @72 h	25	6	19	20	21	23

Table 2. Cross-omics promoter DNA methylation at companion-layer genes (72 h).

Promoter methylation (TSS ± 2 kb) for the loci cited in Section 2.5. Δβ stress = stressed minus unstressed control; treatment columns are relative to the stressed control.

Module	Gene	β unstressed	β stressed	Δβ stress	Δβ QMR	Δβ Secretome	Δβ QMR+Sec
Antioxidant/NRF2	GCLC	0.384	0.44	0.056	0.013	-0.019	-0.041
Antioxidant/NRF2	HMOX1	0.736	0.791	0.054	-0.041	-0.033	0.001
Antioxidant/NRF2	GCLM	0.484	0.525	0.041	-0.007	-0.03	-0.01
Antioxidant/NRF2	TXNRD1	0.725	0.748	0.024	-0.016	-0.05	-0.029
Antioxidant/NRF2	PRDX1	0.694	0.727	0.033	-0.007	-0.032	-0.033
Antioxidant/NRF2	GSTM1	0.695	0.738	0.043	-0.137	-0.044	-0.006
Antioxidant/NRF2	GSTM5	0.836	0.759	-0.078	-0.036	0.067	0.057
Inflammation/Senescence	NFKB1	0.404	0.349	-0.054	0.044	0.05	0.05
Inflammation/Senescence	NLRP3	0.719	0.669	-0.051	0.036	0.019	0.03
Epi_machinery	DNMT1	0.779	0.702	-0.076	0.031	0.042	0.01
Epi_machinery	DNMT3B	0.792	0.846	0.054	-0.019	0.021	-0.008
Epi_machinery	IDH2	0.593	0.651	0.058	0.017	0.031	-0.026
AMD/RPE	CFH	0.683	0.737	0.054	0.014	0.014	-0.034
AMD/RPE	HTRA1	0.868	0.913	0.045	-0.01	-0.058	-0.002
ncRNA_host	NEAT1	0.199	0.147	-0.052	-0.073	-0.048	-0.011
ncRNA_host	BASP1	0.585	0.637	0.052	-0.046	-0.055	-0.068
ncRNA_host	ASPH	0.349	0.392	0.043	0.033	-0.015	-0.051
StructuralFidelity	CTDNEP1	0.77	0.814	0.044	0.041	-0.013	0.021

Figures

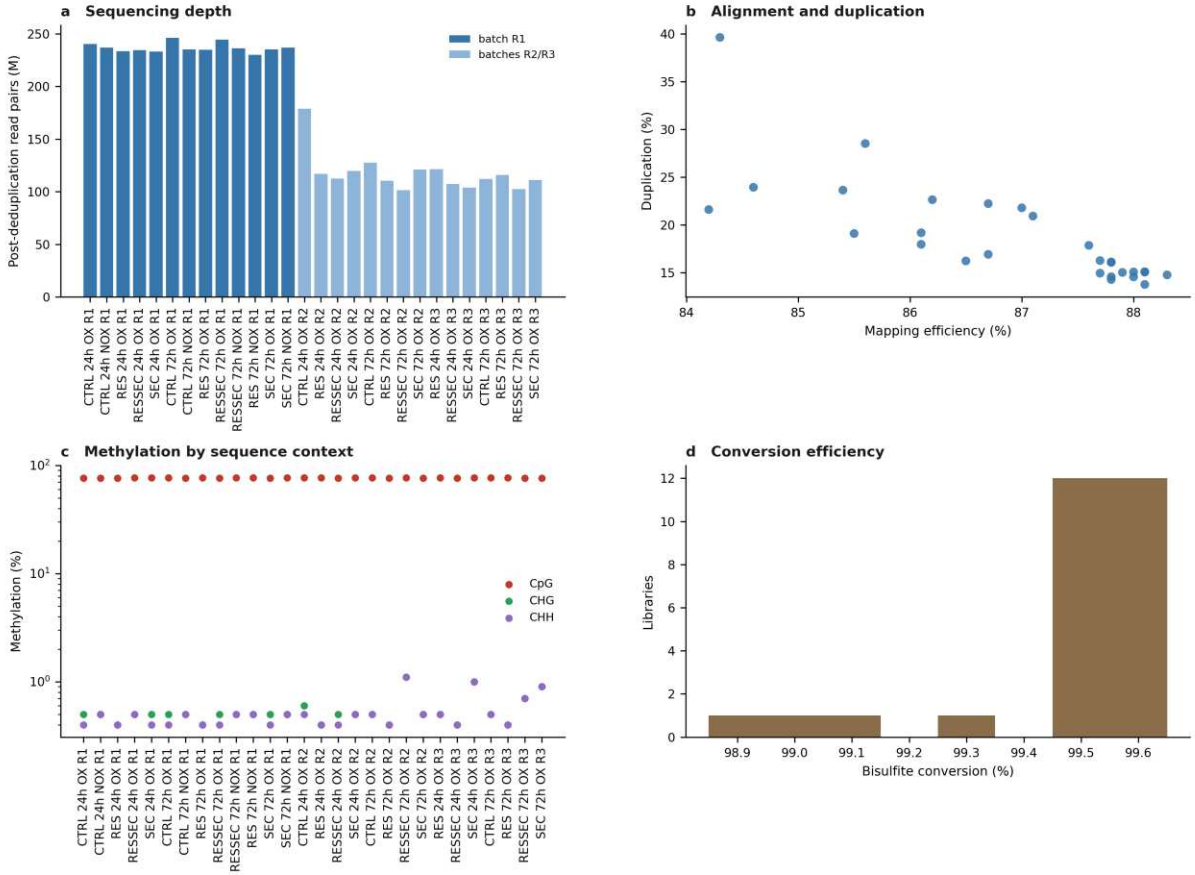

Figure 1. Whole-genome bisulfite sequencing quality control across the 28 libraries. (a) Sequencing depth per library. (b) Mapping efficiency versus duplication rate. (c) Methylation by sequence context (CpG, CHG, CHH; log scale). (d) Distribution of bisulfite-conversion efficiency, estimated from non-CpG methylation. n = 28 libraries; per-library values in Table S1.

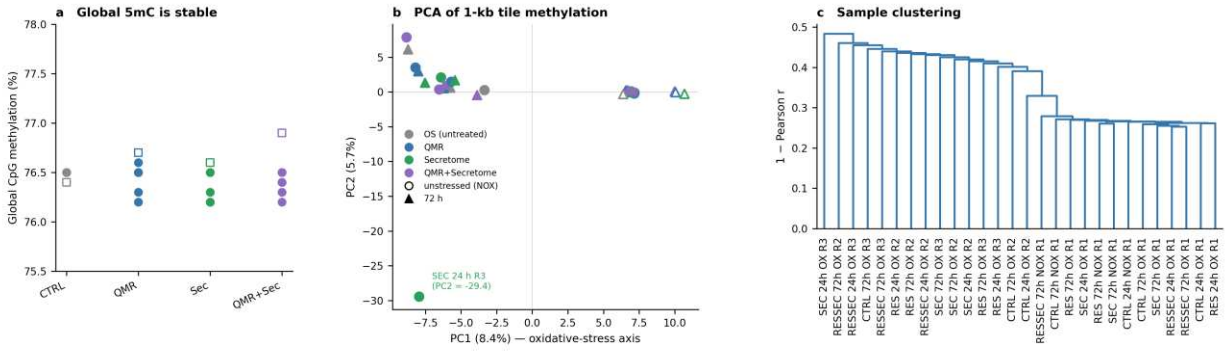

Figure 2. Multivariate structure of the RPE methylome. (a) Global CpG methylation by condition and time point. (b) Principal-component analysis of the 50,000 most variable 1-kb tiles; filled symbols, oxidatively stressed (OX); open symbols, unstressed (NOX); the sample annotated at PC2 = −14.3 is a single secretome replicate at 24 h and is retained in all analyses.

(c) Average-linkage hierarchical clustering on 1 − Pearson r; the primary split separates batch R1 from batches R2/R3. n = 28 libraries.

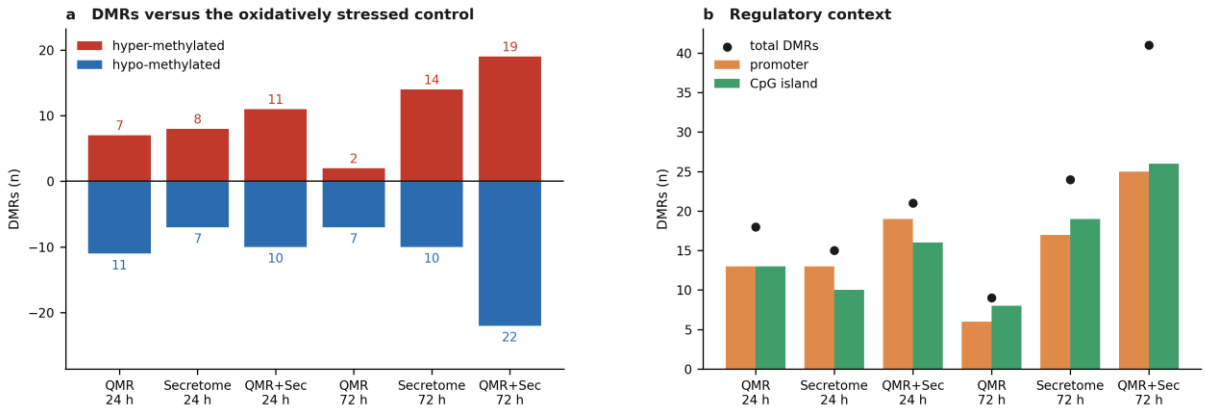

Figure 3. Differential methylation induced by QMR, the secretome and their combination versus the oxidatively stressed control. (a) Numbers of hyper- and hypo-methylated DMRs per contrast (FDR < 0.05, |Δβ| ≥ 0.10; edgeR quasi-likelihood F-test with batch adjustment, three biological replicates per group). (b) Regulatory context of the same DMRs. Counts are given in Table 1.

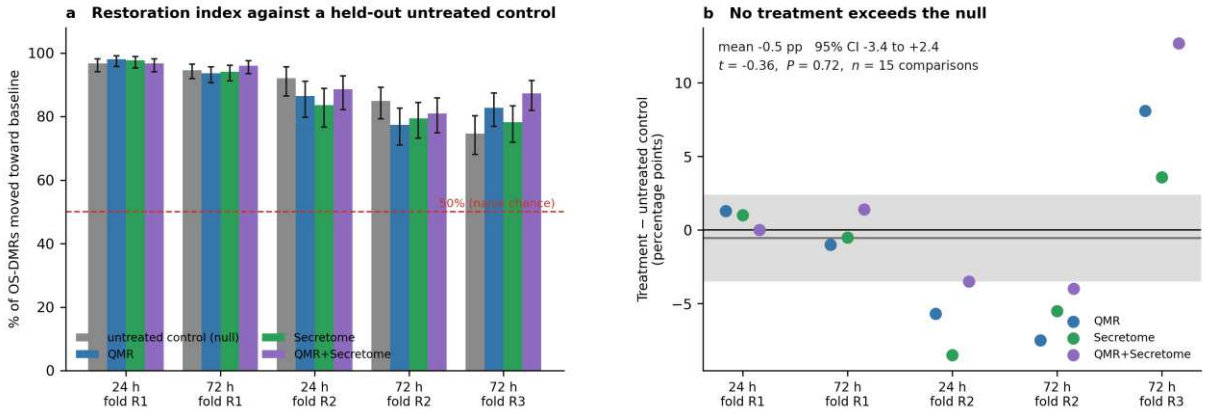

Figure 4. The epigenetic-restoration index against its empirical null. (a) Percentage of oxidative-stress-responsive regions moved toward the unstressed baseline, for each treatment and for a withheld, untreated oxidatively stressed control replicate scored identically; bars are per leave-one-out fold, error bars are 95% Wilson intervals, and the dashed line marks the 50% naive chance expectation. (b) Difference between each treatment and the withheld untreated control; the shaded band is the 95% confidence interval of the mean across all comparisons. No treatment exceeds the null (mean −0.5 percentage points, 95% CI −3.4 to +2.4; one-sample t-test t = −0.36, P = 0.72, n = 15 comparisons). Per-fold values in Table S3c.

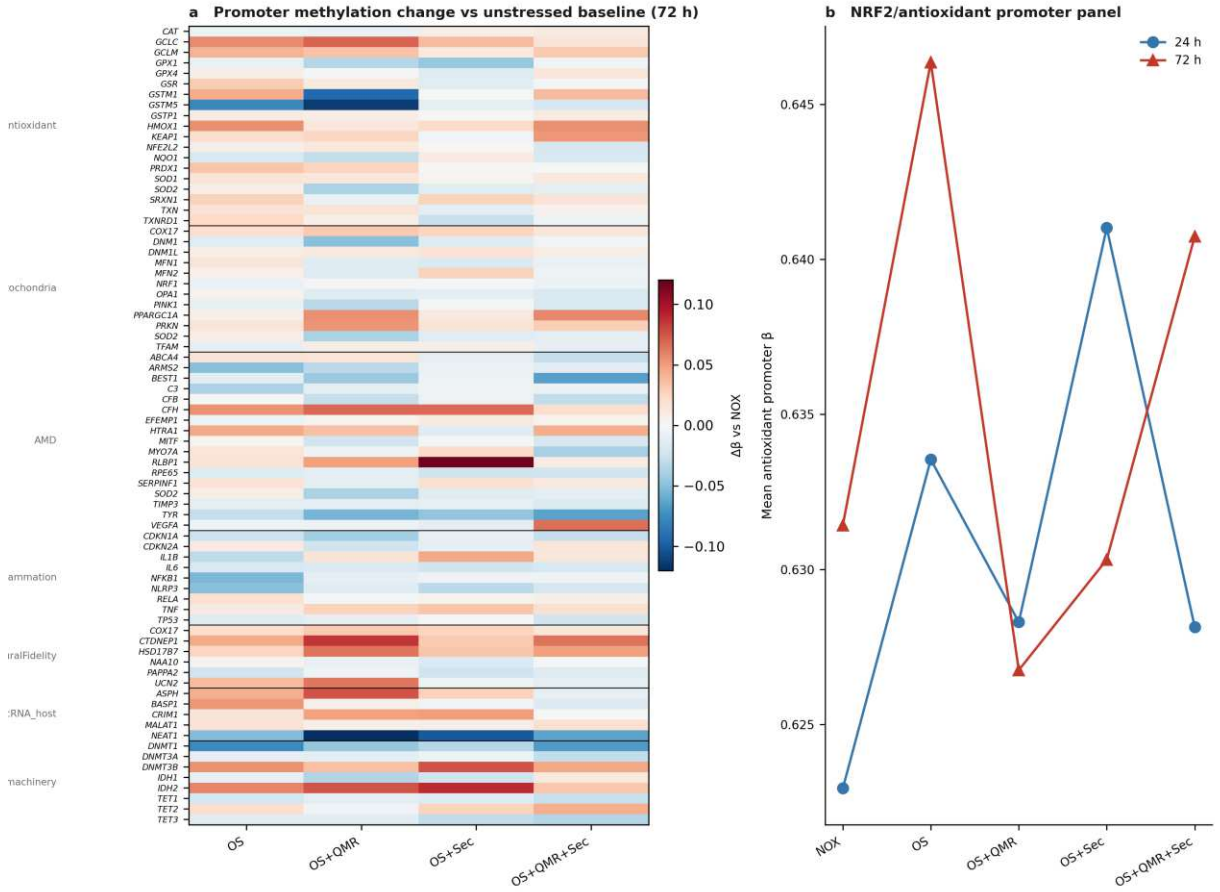

Figure 5. Cross-omics convergence. (a) Promoter methylation change relative to the unstressed baseline at companion-layer genes (72 h). (b) Mean methylation across the NRF2/antioxidant promoter panel (19 genes) by condition and time point. Values in Table 2 and Table S4.

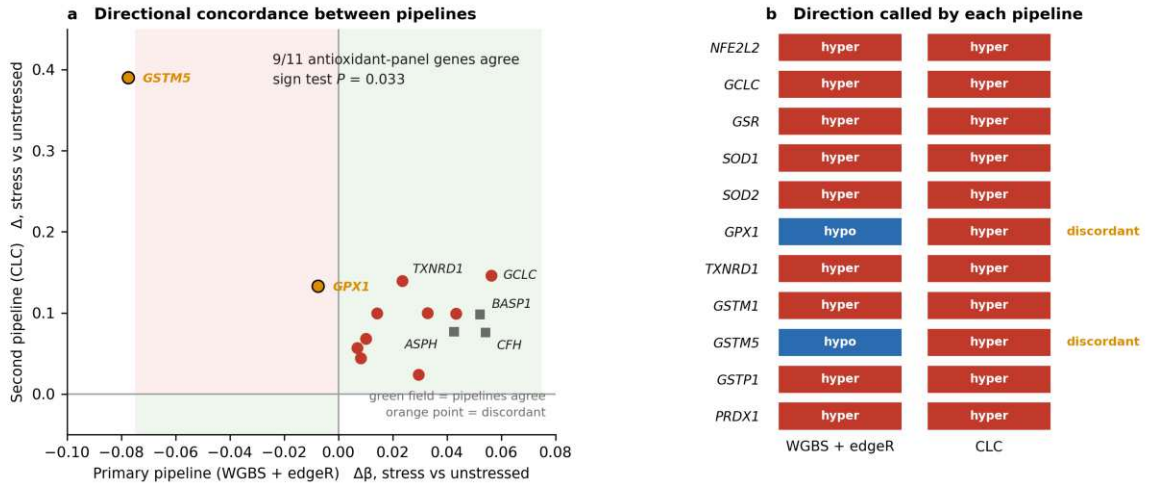

Figure 6. Directional concordance between the two analytical pipelines. (a) Stress-induced methylation change at antioxidant-panel genes in the primary pipeline (WGBS + edgeR, Δβ) against the second pipeline (CLC, Δ); the green field marks agreement in direction, orange points mark the two discordant loci. (b) Direction called by each pipeline per gene. Concordance is 9 of 11 antioxidant-panel genes (exact sign test, P = 0.033). Both pipelines analyse the same batch-R1 libraries; values in Table S5b.

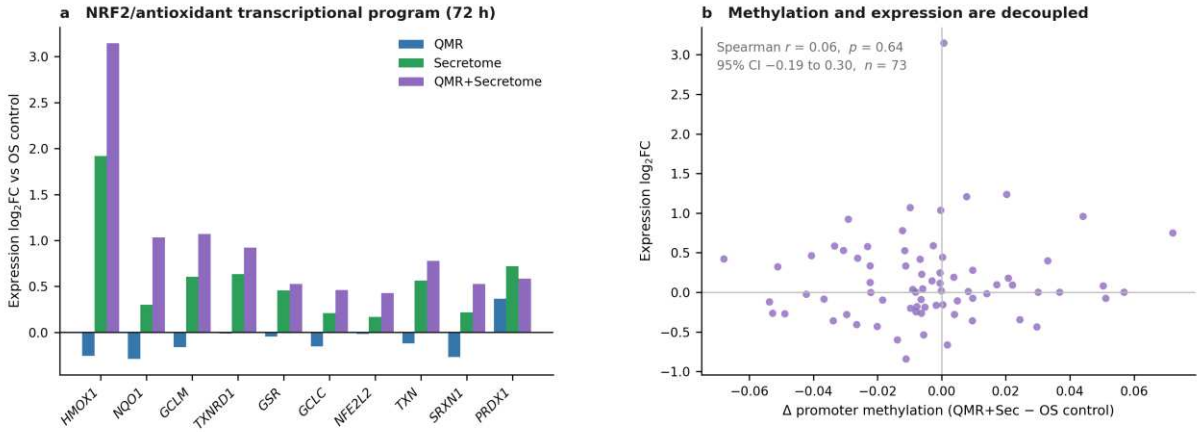

Figure 7. Integration with the matched transcriptome (GEO GSE328981). (a) Expression log2 fold change versus the oxidatively stressed control at 72 h for the NRF2/antioxidant program. (b) Promoter methylation change against expression change across the companion-gene panel (Spearman r = 0.06, p = 0.64, 95% CI −0.19 to 0.30, n = 73 genes).

Supplementary Files

This is a list of supplementary files associated with this preprint. Click to download.

- S1QCperlibrary.tsv
- S3crestorationempiricalnull.tsv
- S3restorationsummary.tsv
- S4crossomicspromotermethylation.tsv
- S2DMRsummary.tsv
- S3bOSsignatureedgeR.tsv
- S5btwopipelineconcordance.tsv
- S2bDMthresholds.tsv
- S6methylationexpressionintegration.tsv
- S5CLCmarqueevalidation.txt